8590–8604 *Nucleic Acids Research, 2018, Vol. 46, No. 16* *Published online 31 May 2018*
doi: 10.1093/nar/gky465

Structural insights into *Drosophila*-C3PO complex assembly and 'Dynamic Side Port' model in substrate entry and release

Xiaobing Mo[1], Xia Yang[2] and Yuren Adam Yuan[1,2,3,*]

[1]Department of Biological Sciences and Centre for Bioimaging Sciences, National University of Singapore, 14 Science Drive 4, Singapore 117543, Singapore, [2]Temasek Life Sciences Laboratory, National University of Singapore, Singapore 117604, Singapore and [3]National University of Singapore (Suzhou) Research Institute, 377 Lin Quan Street, Suzhou Industrial Park, Jiangsu 215123, China

Received February 11, 2018; Revised April 25, 2018; Editorial Decision May 10, 2018; Accepted May 17, 2018

ABSTRACT

In *Drosophila* and human, component 3 promoter of RISC (C3PO), a heteromeric complex, enhances RISC assembly and promotes RISC activity. Here, we report crystal structure of full-length *Drosophila* C3PO (E126Q), an inactive C3PO mutant displaying much weaker RNA binding ability, at 2.1 Å resolution. In addition, we also report the cryo-EM structures of full-length *Drosophila* C3PO (E126Q), C3PO (WT) and SUMO-C3PO (WT, sumo-TRAX + Translin) particles trapped at different conformations at 12, 19.7 and 12.8 Å resolutions, respectively. Crystal structure of C3PO (E126Q) displays a half-barrel architecture consisting of two Trax/Translin heterodimers, whereas cryo-EM structures of C3PO (E126Q), C3PO (WT) and SUMO-C3PO (WT) adopt a closed football-like shape with a hollow interior cavity. Remarkably, both cryo-EM structures of *Drosophila* C3PO (E126Q) and *Drosophila* SUMO-C3PO (WT) particles contain a wide side port (∼25 Å × ∼30 Å versus ∼15 Å × ∼20 Å) for RNA substrate entry and release, formed by a pair of anti-parallel packed long α1 helices of TRAX subunits. Notably, cryo-EM structure of SUMO-C3PO showed that four copies of extra densities belonging to N-terminal SUMO tag are located at the outside shell of SUMO-C3PO particle, which demonstrated that the stoichiometry of TRAX/Translin for the *in vitro* expressed and assembled full-length *Drosophila*-SUMO–C3PO particle is 4:4, suggesting *Drosophila* C3PO is composed by TRAX/translin at a ratio of 4:4. Remarkably, the comparison of the cryo-EM structures suggests that the C3PO side ports regulated by α1 helices of TRAX molecules are highly dynamic. Hence, we propose that C3PO particles could adopt a 'Dynamic Side Port' model to capture/digest nucleic acid duplex substrate and release the digested fragments through the dynamic side ports.

INTRODUCTION

In eukaryotes, small RNA processing is an RNA-centered multiple-step maturation process, which is processed by different RNA-protein complexes (1). Among them, RNA-induced silencing complex (RISC) is the effector module in RNA interference (RNAi) pathway, whose activation is triggered by cleavage and release the passenger strand of the bound small interfering RNA (siRNA) and microRNA/* duplex by the Argonaute protein (Ago), the catalytic engine of the RISC (2–7). Consequently, the activated RISC, an Ago with the intact guide strand imbedded inside, degrades the paired mRNA targets to cause gene silencing (8–11). In literature, many RNA-binding proteins are reported to participate in small RNA duplex loading into RISC, passenger strand digestion and release (8,12–15). In human and *Drosophila*, C3PO (Translin-TRAX complex) was reported to participate in RISC activation by removing the nicked passenger strand cleaved by Ago (16,17). In prokaryotes, C3PO-like molecules with unknown biological functions were discovered based on sequence similarities and *in vitro* cleavage activities (18–20). The crystal structures of truncated *Drosophila*-C3PO at 3.4 Å resolution, human-C3PO at 2.9 Å resolution, *Archaeoglobus fulgidus* C3PO in complex with 14 bp dsRNA at 2.9 Å resolution and *Nanoarchaeum equitans* C3PO in complex with ssRNA at 2.1 Å resolution were determined (8,21–23). In addition, negative-stained EM structure of full-length *Drosophila* C3PO at ∼15 Å resolution and cryo-EM structure of human-C3PO at ∼15 Å resolution were also reported (23). Notably, all the full-length C3POs adopt closed football-shaped structures, which are very similar to previous reported Translin homo-octamer structures (8,21,22,24). Strikingly, *in vitro*

*To whom correspondence should be addressed. Tel: +65 65162724; Email: dbsyya@nus.edu.sg

mass-spectrometric analysis of *Drosophila* C3PO revealed a mixture of ratios of 2:6 and 3:5 (TRAX:Translin) in C3PO, which was partially supported by the reported *N. equitans* C3PO (*Ne*-C3PO) structure (21,23). In addition, human-C3PO structures showed that the two catalytic TRAX subunits were packed side-by-side in a head-to-tail mode, with the active residues facing into the concaved interior cavity (21). By contrast, *Archaeoglobus fulgidus* C3PO (*Af*-C3PO) in complex with 14 bp dsRNA revealed a symmetric fold with the bound RNA duplex encapsulated within the inner cavity of *Af*-C3PO (24).

Although these complex structures provide important insights into RNA substrate binding and cleavage within C3PO, the structural mechanism of RNA substrate entry and release out of C3PO remains largely unknown. In literature, 'conformational shift' and 'dissociation and reassembly' models were proposed to explain the substrate entry and release by C3PO and C3PO-like octamer (21,24,25). The 'conformational shift' model was supported by the structural comparison of *Ne*-C3PO octamer with and without ssRNA substrate, which reveals a structural gap as the consequence of structural rearrangement of the long α1-helices of the packed TRAX subunits (21). The 'dissociation and reassembly' model was partially supported by the observation of human Translin tetramers in solution by introduction of a single mutation to disrupt nucleic acids binding ability (26).

To minimize the disturbance of C3PO assembly by junk nucleic acids expressed together with C3PO during the *in vitro* expression system and determine the *Drosophila*-C3PO structures authentically mimicking C3PO conformations with and without RNA binding, we have screened the RNA binding affinities of several inactive C3PO mutants, including E123Q, E126Q and D204N. We found *Drosophila*-C3PO (E126Q) displays much more compromised RNA binding affinities towards both RNA duplex and ssRNA. Hence, both *Drosophila*-C3PO (E126Q) and *Drosophila*-C3PO (WT) were used for structural determination.

To investigate the structural insights into C3PO assembly and substrate entry and release, we have determined the high-resolution crystal structure of *Drosophila*-C3PO (E126Q) at 2.1 Å resolution, cryo-EM structure of *Drosophila*-C3PO (E126Q) at ∼19.7 Å resolution and cryo-EM structure of *Drosophila*-C3PO (WT) at 12 Å resolution. To validate the structural feature and stoichiometry of TRAX–Translin ratio, we have also determined the cryo-EM structure of *Drosophila*-SUMO-C3PO (SUMO-TRAX + Translin, WT) at 12.8 Å resolution. Surprisingly, the crystal structure of *Drosophila*-C3PO (E126Q), an RNA binding deficient mutant, displays a half-barrel architecture consisting of two Trax/Translin heterodimers, whereas cryo-EM structures of *Drosophila*-C3PO (E126Q), *Drosophila*-C3PO (WT) and *Drosophila*-SUMO-C3PO (WT) in solution adopt a closed football-like shape with a hollow interior cavity. Remarkably, cryo-EM structures of both C3PO (E126Q) and SUMO-C3PO (WT) particles contain a wide side port (∼25 Å × ∼30 Å and ∼15 Å × ∼20 Å, respectively) regulated by the two anti-parallel packed long α1 helices of TRAX subunits. Notably, in crystal structure of *Drosophila*-C3PO (E126Q) tetramer, two Translin subunits are located in the middle of the C3PO (E126Q) tetramer, comprising the most convex outer surface. Two TRAX subunits are located edgewise, comprising the most concave interior surface. These two TRAX subunits are ∼20 Å distance away and no interactions between them are observed. Structural docking of the two *Drosophila*-C3PO (E126Q) tetramers into the cryo-EM maps, based on the unique secondary structure of TRAX (the long loop between α4 and α5), indicates that the closed football-like *Drosophila*-C3PO octamer could be assembled by two tetramers comprising four TRAX–Translin heterodimers with the TRAX subunits packed in a head-to-tail mode. Hence, the anti-parallel packed long α1 helices of TRAX subunits could serve as a regulating gate to open and close the side ports from both sides. Moreover, the C3PO inner chamber is bigger enough to accommodate two 14 bp RNA duplex simultaneously.

Consistently, cryo-EM structure of SUMO-C3PO demonstrates that four copies of extra densities corresponding to N-terminal SUMO tag are located at the outside shell of SUMO-C3PO particle and next to the observed side-ports, which further confirms that the stoichiometry of TRAX/Translin within the *in vitro* expressed and assembled *Drosophila-C3PO* particle is 4:4.

Hence, we speculate that C3PO particles could adopt a 'Dynamic Side Port' model to capture/digest nucleic acid duplex substrate and release the digested fragments through the dynamic side ports.

MATERIALS AND METHODS

Cloning, protein expression and purification of *Drosophila*-C3PO complex

Both open reading frame (ORF) of *Drosophila* Translin and Trax were amplified by DNA polymerase and sub-cloned into a pET-Duet-1 vector. The constructed expression plasmid (co-expressing N-His-tagged Trax and non-tagged Translin) was transformed into *Escherichia coli* BL21 (DE3) for co-expression. The cells were grown in LB media supplemented with Ampicillin antibiotics to an OD_{600} value reaching 0.6; a final concentration of 0.4 mM IPTG was added to induce the recombinant protein expression. Cells were cultured overnight and harvested by centrifugation. The pellets were resuspended in lysis buffer containing 20 mM Tris (pH 7.4), 500 mM NaCl, 1 mM DTT and 2 mM EDTA and disrupted by homogenizer for four times. After ultracentrifugation at 40 000 rpm for 1 h, the supernatant was collected and purified by Histidine affinity chromatography column, followed by gel filtration chromatography column. The final C3PO protein was dialyzed against a buffer containing 500 mM NaCl, 25 mM Tris 7.4 and subsequently concentrated to 12 mg/ml. The *Drosophila*-C3PO (E123Q), C3PO (E126Q) and C3PO (D204N) mutant constructs were made using QuickChange site directed mutagenesis kit and verified by sequencing. The mutant proteins were prepared using the similar approaches for wild type C3PO purification. The *Drosophila*-SUMO-C3PO (WT) construct was modified from the *Drosophila*-C3PO (WT) construct by insertion, in frame, of a SUMO tag at 5′- of TRAX gene. The *Drosophila*-SUMO-C3PO (WT) protein was prepared and purified using similar approaches for wild type C3PO. Selenomethionine (Se-Met)-substituted *Drosophila*-C3PO

(E126Q) was prepared using a method described previously (Doublié, 1997).

Electrophoresis mobility shift assay (EMSA)

Gel mobility shift assays were performed to detect RNA binding ability of *Drosophila*-C3PO proteins. Purified *Drosophila*-C3PO (WT, E123Q, E126Q and D204N) were mixed, respectively, with biotin-labeled target RNAs in a buffer containing 20 mM HEPES (pH 7.5), 100 mM NaCl, 1 mM DTT and 2 mM EDTA, and incubated at 37°C for 10 min. Samples containing C3PO-RNA were run on 5% polyacrylamide native gels at 100 V for 30 min. The resolved RNA was transferred and electro-blotted onto a Hybond-N+ membrane. After cross-link by UV, detection was performed according to the instruction of Light Shift Chemiluminescent EMSA kit (Thermo Fisher Scientific Inc., USA). The EMSA image was collected on the G-Box biomolecular imager (GE Healthcare).

Crystallization and structure determination

The concentrated *Drosophila*-C3PO (E126Q) was submitted for crystallization trials by hanging drop method in 24-well trays. More than 500 conditions were screened and the best crystals were grown at 20°C by mixing 1.0 μl of protein with 1.0 μl of reservoir containing 15% MPD and 100mM sodium acetate (pH 5.0) and equilibrated over 1 ml of reservoir solution for a course of 3 days. After optimization, single crystals (maximum size of 0.3 mm × 0.3 mm × 0.2 mm) were picked and flash frozen (100 K) in the above reservoir solution supplemented with 30% glycerol. Three sets of 360 frames with 1° oscillation at wavelengths of 0.9789 Å (peak), 0.9792 Å (inflection) and 0.9540 Å (remote) were collected on one single *Drosophila*-C3PO (E126Q) crystal. The data were processed and scaled by HKL2000 (www.hkl-xray.com). The structure of *Drosophila*-C3PO (E126Q) was determined by SOLVE/RESOLVE (http://www.solve.lanl.gov) using multiple wavelength anomalous dispersion method (27). The model was built by using the program O (http://xray.bmc.uu.se/alwyn) and refined using REFMAC/CCP4 (www.ccp4.ac.uk). The crystallographic statistic details of these structures are listed in Table 1. The structural figures were produced and the electrostatics was calculated using PyMOL (Delano Scientific).

Cryo electron microscopy (Cryo-EM)

5 μl purified *Drosophila*-C3PO (E126Q), *Drosophila*-C3PO (WT) or *Drosophila*-SUMO-C3PO (WT) (1 mg/ml) specimen was loaded onto a Quatifoil 2/1 grid, blotted with filter papers (two times, 2 seconds per blotting) and rapidly plunged into liquid ethane, pre-cooled by liquid nitrogen. Cryo-EM images were taken from the frozen grids in a Tecnai T12 TEM cryo electron microscope operated at 120 kV, with a magnification of 67 000 and a pixel size of 1.18 Å/pixel. Measured defocus values of these images range from –2 μm to –5 μm.

Approximately 30 000 individual particles for wild type *Drosophila*-C3PO were excised from micrographs by boxing and the contrast transfer function (CTF) correction for each micrograph was determined based on incoherently averaged Fourier transforms of each image by EMAN2 (blake.bcm.tmc.edu/EMAN2). The particle sets were built and averaged. Only the good average classes with apparent complex formation were subjected to make initial models by the application of d2 symmetry. Roughly 15 600 particles were used for 3D reconstruction using EMAN2 software. The final effective resolution of the map is ∼12 Å, when 0.143 Fourier correlation criterions are used. The densities of C3PO were extracted from the density map, and visualized using UCSF Chimera software (www.cgl.ucsf.edu/chimera).

In parallel, approximately 5,600 and 13,200 individual particles were collected for *Drosophila*-C3PO (E126Q) and *Drosophila*-SUMO-C3PO (WT), respectively, in a Tecnai 12 TEM cryo electron microscope operated at 120 kV, with a magnification of 67 000 and a pixel size of 1.69 Å/pixel. Measured defocus values of these images range from –2 μm to –5 μm. The final effective resolutions of the maps are ∼19.7 Å and 12.8 Å for *Drosophila*-C3PO (E126Q) and *Drosophila*-SUMO-C3PO (WT) respectively, when 0.143 Fourier correlation criterion is used.

Table 1. Data collection, phasing, and refinement statistics

	Drosophila C3PO
Space group	$C222_1$
PDBID	3AXJ
Wavelength (Å)	0.97893
Cell dimensions	
a (Å)	101.68
b (Å)	114.72
c (Å)	113.91
Molecule/ASU	1 TRAX–Translin heterodimer
Resolution (Å)[a]	2.10 (2.18–2.10)
R_{sym} (%)[a]	6.6 (25.8)
$I/\sigma(I)$	39.0 (4.7)
Completeness (%)[a]	99.9 (100.0)
Redundancy[a]	7.5 (7.3)
FOM (50–2.10)	0.524
Resolution (Å)	
No. reflections	40,056
R_{work} (R_{free}) (%)	20.3 (23.8)
No. atoms	
Protein	3.719
Water	208
B-factors (Å^2)	
Protein	39.36
Water	46.57
R.m.s. deviations	
Bond lengths (Å)	0.015
Bond angles (°)	1.375
% favored (allowed) in Ramachandran plot	94.4 (5.6)

[a]Values for the highest-resolution shell are in parentheses.

RESULTS

Inactive *Drosophila*-C3PO mutants display compromised ssRNA and duplex RNA binding affinities

To assess the binding ability between *Drosophila*-C3PO and ssRNA or duplex RNA in the solution, we performed electrophoretic mobility shift assay (EMSA). As expected, wild type *Drosophila*-C3PO demonstrated strong binding affini-

ties towards both unstructured ssRNA and duplex RNA, in a sequence non-specific manner (Figure 1A and B).

Next, to investigate the impact of the catalytic active residues E123, E126 and D204 in RNA substrate binding and find a *Drosophila*-C3PO mutant deficient of RNA binding ability, we performed EMSA/bio-dot-based EMSA by comparison of the RNA duplex binding abilities among E123Q, E126Q and D204N mutants (Supplementary Figure S1). Surprisingly, E126Q mutant displayed much weaker binding affinity with RNA duplex compared to other catalytic inactive mutants, suggesting the introduction of Q mutation at E126 has significantly compromised binding affinity towards RNA duplex (Figure 1C, Supplementary Figure S2). To further investigate this issue, analytic size exclusion chromatography experiments were performed. As expected, a stable C3PO (WT)-ssRNA complex was achieved, whereas no stable C3PO (E126Q)-ssRNA complex was detected (Figure 1D). Hence, we chose *Drosophila*-C3PO (E126Q) and wild type *Drosophila*-C3PO for structural determination. We speculate that the much weaker RNA binding ability of *Drosophila*-C3PO (E126Q) could minimize the disturbance of *Drosophila*-C3PO assembly by the junk nucleic acids co-purified together with *Drosophila*-C3PO. Therefore, the structures of *Drosophila*-C3PO in complex with RNA and *Drosophila*-C3PO (E126Q) could represent the *Drosophila*-C3PO conformations with and without RNA binding, respectively.

Crystal structure of *Drosophila*-C3PO (E126Q) tetramer

After exhaustive crystallization trials, we were not able to obtain suitable crystals of full-length wild type *Drosophila*-C3PO in complex with RNA substrates. By contrast, full-length *Drosophila*-C3PO (E126Q) protein was crystallized in the space group of $C222_1$, with a unit-cell dimension of $a = 101.68$ Å, $b = 114.72$ Å, $c = 123.91$ Å. The structure was determined by SAD based on the anomalous data collected from the crystal of selenium-methanione labeled *Drosophila*-C3PO (E126Q), with the crystallographic analysis shown in Table 1. There is one Translin/TRAX heterodimer per asymmetric unit and two crystallographic related Translin/TRAX heterodimers form a tightly packed hetero-tetramer (Figure 2A). Notably, both TRAX and Translin molecules are composed of seven α-helices (Figure 2B). Structure superimposition between them reveals a similar fold, a two-layered right-handed super-helical bundle, with an r.m.s.d. of 4.28 Å (216 residues), except TRAX containing 2 more β-strands in the long loop region connecting α4 and α5 (Figure 2C). Disordered regions of TRAX subunit, including loop segments (amino acids aa164-185) and the N-terminal unstructured region (amino acids aa1–22), are not included in the model (Figure 2A). In our structure, TRAX–Translin heterodimer is formed through hydrophobic interactions, formed by some polar and non-polar residues, and the conserved residues for both TRAX and Translin, are located in the TRAX-translin heterodimer interface (Figure 2B). The buried surface area of TRAX–Translin heterodimer is 4,441 $Å^2$ per molecule, suggesting TRAX–Translin heterodimer could be physiologically relevant. By contrast, only few hydrophobic interactions between the two packed Translin long α1 helices are observed (Figure 2D). The topology of the crystal structure of our full-length *Drosophila*-C3PO (E126Q) is almost identical to the published truncated *Drosophila*-C3PO, which has both 29 residues N-terminal truncation and 18 resides C-terminal truncation in TRAX (23). However, our C3PO (E126Q) tetramer assembly is dramatically different from the published hexamer assembly. In our structure, the two TRAX/Translin heterodimers are packed in a head-to-tail mode through the long α1 helices of Translin subunits, the TRAX subunits locate at both sides of the tetramer and interact with Translin subunits, hence no direct interactions between TRAXs are observed (Figure 2A). The two TRAX/Translin heterodimers form a half-barrel cavity with the TRAX active amino acids E123, E126 (mutated to Q in our structure) and D204 forming an acidic patch at the edges of the concaved cavity (Figure 2E). Notably, in our full-length *Drosophila*-C3PO (E126Q) structure, neither Translin–Translin homodimer nor TRAX–TRAX homodimer is observed.

Overall structure of *Drosophila*-C3PO octamer

In literature, different structural arrangements of eukaryotic C3PO were reported (Supplementary Figure S3A–E) (8). Human-C3PO was determined at 2.95 Å resolution, which contains three Translin and one TRAX subunits per asymmetric unit. In human-C3PO structure, a closed football-like shape architecture consisting one TRAX/Translin heterodimer and three Translin/Translin homodimers were generated by 2-fold crystallographic symmetric operation (Supplementary Figure S3A). In our structure, extensive conserved hydrophobic interactions between TRAX–Translin were observed and relatively few interactions between TRAX–TRAX and Translin–Translin were observed (Figure 2D). Notably, in our structure, the buried surface area for TRAX–Translin heterodimer is 4,441 $Å^2$ per molecule, whereas the buried surface areas for the packed TRAX–TRAX and Translin–Translin homodimer are 39.56 and 186.59 $Å^2$ per molecule, respectively, suggesting the TRAX–Translin heterodimer could be the building unit and multiple building arrangements could be existed for C3PO complexes.

In literature, truncated *Drosophila*-C3PO was determined at 3.4 Å resolution, surprisingly, with one TRAX–Translin heterodimer and one Translin monomer per asymmetric unit. An open barrel-like shape architecture consisting one TRAX/Translin heterodimer and two Translin/Translin homodimers were generated by 2-fold crystallographic symmetric operation (Supplementary Figure S3B). In this structure, one Translin homodimer was bracketed by two TRAX–Translin heterodimers at both sides. Notably, the C-terminal truncated residues of Translin and N-terminal truncated residues of TRAX are indeed disordered at our high-resolution full-length *Drosophila*-C3PO (E126Q) crystal structure, suggesting these residues should not play the critical roles in changing the structural arrangement of *Drosophila*-C3PO from octameric fold to hexameric fold. Furthermore, our high-resolution crystal structure of full-length *Drosophila*-C3PO (E126Q) adopts a tetrameric fold instead of hexameric or octameric fold (Supplementary Figure S3C). Hence, we speculate that although the conserved

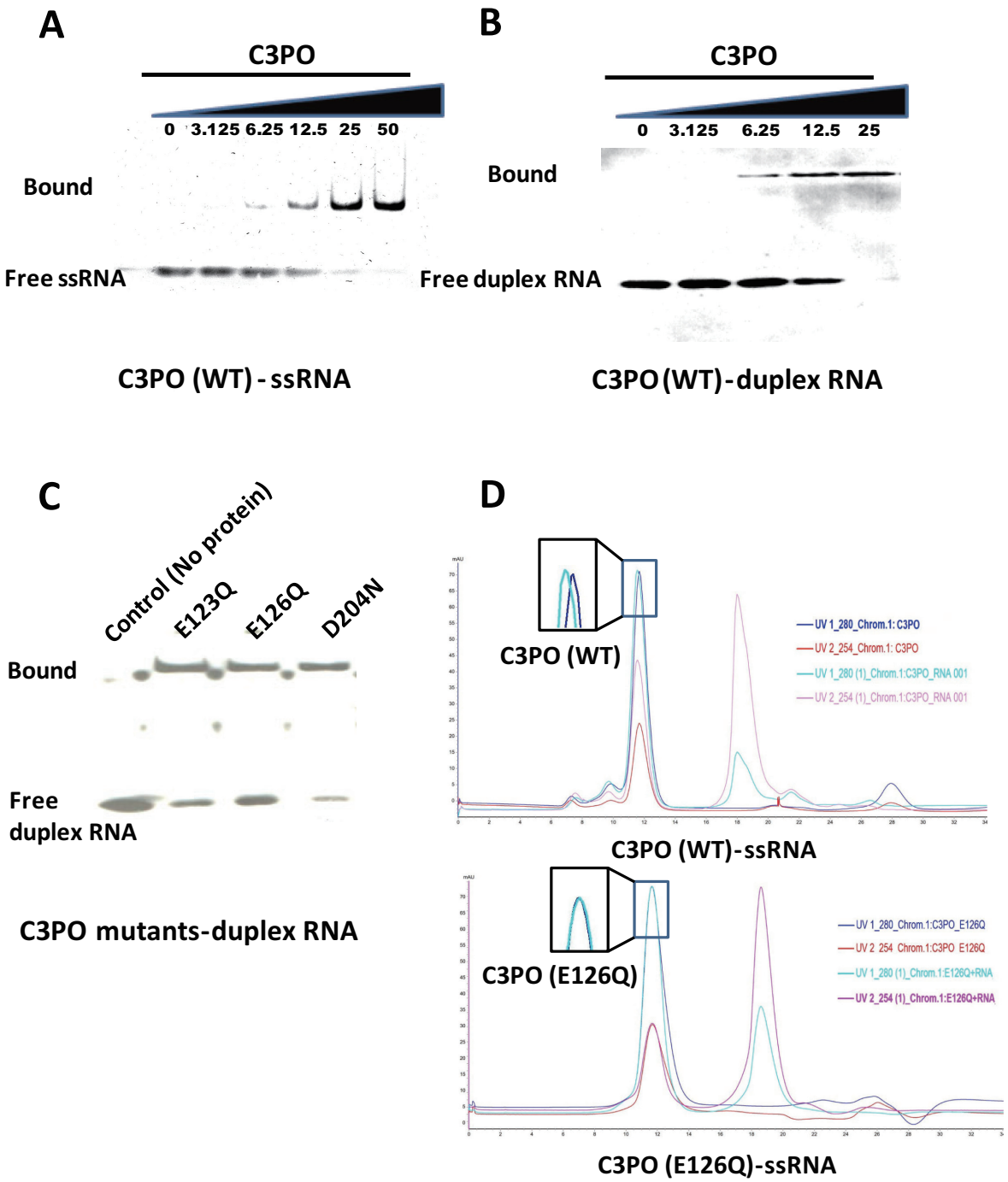

Figure 1. RNA binding abilities of full-length *Drosophila*-C3PO and its mutants. (**A**) Electrophoretic mobility shift assay (EMSA) on full-length *Drosophila*-C3PO binding to ssRNA. (**B**) Electrophoretic mobility shift assay (EMSA) on full-length *Drosophila*-C3PO binding to duplex RNA, in which 2-fold titration of full-length from 2 to 20 μM were incubated with 2 nM biotin-labeled nucleic acids at 37°C for 30 min. (**C**) Electrophoretic mobility shift assay (EMSA) on inactive full-length *Drosophila*-C3PO mutants binding to duplex RNA. (**D**) Upper panel: Size exclusion chromatography of wide type (WT) full-length *Drosophila*-C3PO binding to duplex RNA. The up-field shift of the curve (blue curve versus black curve) indicates the formation of stable complex of full-length *Drosophila*-C3PO (WT) in complex with duplex RNA (inserted figure). Lower panel: Size exclusion chromatography of full-length *Drosophila*-C3PO (E126Q) binding to duplex RNA. The non-shift of the curve (blue curve versus black curve) indicates the failure of formation of stable complex of full-length *Drosophila*-C3PO (E126Q) in complex with duplex RNA (inserted figure).

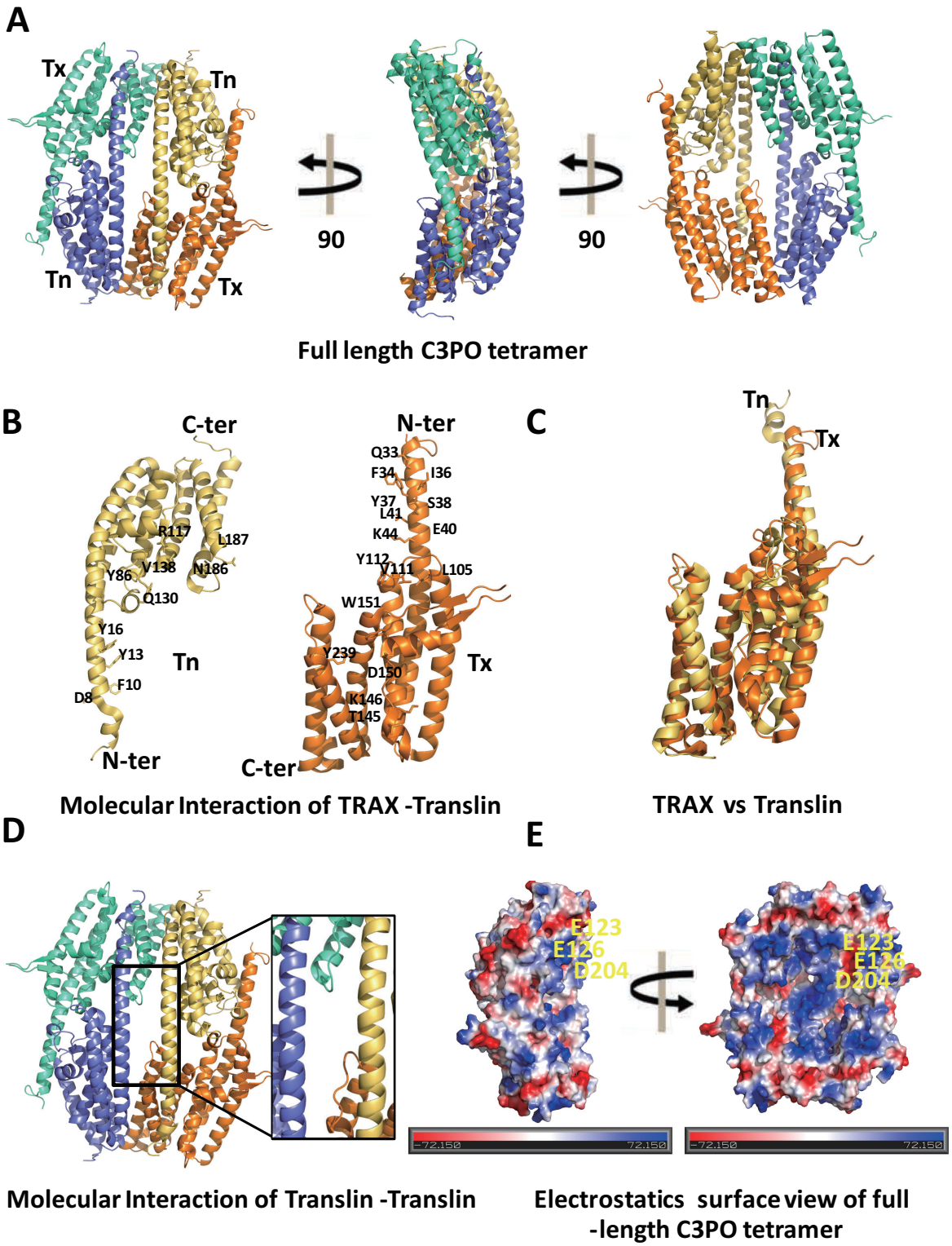

Figure 2. Crystal structure of full-length *Drosophila*-C3PO tetramer. (**A**) Cartoon representation of crystal structure of full-length *Drosophila*-C3PO. C3PO adopts a half barrel tetramer formed by two TRAX–Translin heterodimers packed by Translin–Translin subunits. The first TRAX–Translin heterodimer is labeled in green (TRAX) and blue (Translin) respectively, whereas the second TRAX–Translin heterodimer is labeled in orange (TRAX) and yellow (Translin) respectively. (**B**) Close-up view of extensive interactions between TRAX–Translin heterodimer. The side chains of the conserved interaction residues are indicated. (**C**) Structural superimposition of TRAX with Translin subunits. TRAX and Translin subunits are labeled in orange and yellow, respectively. (**D**) Molecular interactions between Translin–Translin subunits among the C3PO tetramer. (**E**) Vacuum electrostatics surface view of the inner concave of full-length *Drosophila*-C3PO tetramer, in which the blue and red color represent the positive and negative potential residues, show continuous negative patches within the C3PO inner cavity. The catalytic active residues, E123, E126Q and D204, are indicated as the same views of the first panels of Figure 2A.

TRAX–Translin heterodimer repeatedly observed from all the C3PO structures is indeed physiologically relevant, the different oligomeric arrangements observed from different crystal structures could be significantly influenced by crystal packing.

Cryo-EM structures of full-length *Drosophila*-C3PO (E126Q), *Drosophila*-C3PO (WT) and *Drosophila*-SUMO-C3PO (WT)

To explore the structural basis for *Drosophila*-C3PO assembly, we have screened the cryo-EM images of *Drosophila*-C3PO (WT) with and without RNA substrate, *Drosophila*-C3PO (E126Q) without RNA substrate and *Drosophila*-SUMO-C3PO (WT) without RNA substrate. At the end, we were able to reconstruct the 3D structures of *Drosophila*-C3PO (E126Q), *Drosophila*-C3PO (WT) and *Drosophila*-SUMO-C3PO (WT) at free form. However, we were not able to reconstruct 3D structure of *Drosophila*-C3PO (WT) in complex of RNA duplex due to aggregation of the particles under cryo-EM condition. Nevertheless, we managed to collect ∼5600 C3PO (E126Q) particles and reconstructed the C3PO (E126Q) 3D structure to a resolution at ∼19.7 Å (FSC ∼ 0.143). As expected, full-length *Drosophila*-C3PO (E126Q) in solution adopts a football-like octameric fold, which could comprise two copies of tetramers derived from our crystal structure. Astonishingly, we observed a huge side port (∼25 Å × ∼30 Å) at the 2D average images and the reconstructed 3D structure (Figure 3A–C). Although at ∼19.7 Å resolution, it was difficult to precisely dock the crystal structures into the cryo-EM structure of C3PO (E126Q), we managed to dock the crystal structure into the map due to the unique structural loop between α4 and α5 of TRAX subunits. In our docked model, C3PO (E126Q) forms octamer with two TRAX subunits lining the side port (Figure 3D). Notably, such structural arrangement leaves the acid patch of the active sites right next to the side port so that the single-stranded RNA substrates could reach the active sites without dissociation and re-assembly of C3PO (Figure 3C–D).

To further explore whether or not the dynamic side port could be the results of structural breath and/or the introduction of E126Q to TRAX molecule, we have collected ∼15 600 C3PO (WT) particles for 3D structure reconstruction. Remarkably, ∼95% of C3PO (WT) particles adopt the closed conformation, whereas only 5% of C3PO (WT) particles adopt the open conformation. We were able to reconstruct the 3D structure of C3PO (WT) particles at the closed conformation to a resolution at ∼12 Å (FSC ∼ 0.143) (Figure 4A and B). In this closed conformation, no side port was observed at either the reconstructed 3D structure or the 2D average images (Figure 4A and C). By contrast, an initial 3D structure model of C3PO (WT) particles based on the ∼5% data clearly showed a side port (Supplementary Figure S4), which is similar to the reconstructed 3D structure of C3PO (E126Q) particles trapped at open conformation.

Based on the reconstructed EM map at ∼12 Å resolution without distortion, we were able to almost precisely dock our X-ray structure into the C3PO electron density map by taking advantage of the characteristic two-layered α-helical bundles and the unique loop region between the α4 and α5 of TRAX. The docked model clearly showed that the two half concaved tetramers packed together to form an octameric C3PO complex. Visual inspection of electron microscopy density map of the wild type full-length *Drosophila*-C3PO suggested the presence of four Translin-TRAX heterodimers aligning in a head-to-tail mode (Figure 4D, Supplementary Figure S5), which is against the ratio of TRAX–Translin derived from published structures.

Notably, in our docked model, the N-termini of TRAX subunits are located at the surface of the particle, which prompted us to validate our docked model and the TRAX–Translin ratio by determining cryo-EM structure of C3PO with N-terminal TRAX labeled. Hence, we decided to determine the structure of N-terminal SUMO tagged C3PO particle (SUMO-TRAX + Translin) and expected the location and the copy number of SUMO molecules should provide the direct evidence for the exact ratio of TRAX–Translin. Therefore, to further investigate the stoichiometry ratio of TRAX–Translin within the *in vitro* expressed and assembled *Drosophila* C3PO particle in solution, we expressed and purified N-terminal SUMO-tagged C3PO, collected 13,200 *Drosophila*-SUMO-C3PO (WT) particles and reconstructed the 3D structure of *Drosophila*-SUMO-C3PO (WT) to a resolution at ∼12.8 Å (FSC ∼ 0.143) (Figure 5A and B). As expected, cryo-EM structure of the full-length *Drosophila* SUMO-C3PO clearly showed that four copies of extra densities belonging to N-terminal SUMO tag are located at the outside shell of SUMO-C3PO particle (Figure 5C), which demonstrated that the stoichiometry of TRAX/Translin for the *in vitro* expressed and assembled full-length *Drosophila*-C3PO particle is 4:4.

STRUCTURAL MODEL OF *Drosophila*-C3PO PARTICLE IN COMPLEX WITH RNA SUBSTRATE

Multiple octameric structures of C3PO, C3PO-like and Translin were determined at different resolutions by either X-ray crystallography or cryo-EM (8,21–24,28,29). All these structures assemble into a very similar closed football-like shape. Among them, the homo-octameric *Af*-C3PO and the *Ne*-C3PO were determined in complex with dsRNA and ssRNA, respectively (21,24). Notably, asymmetric octameric arrangement was observed in *Ne*-C3PO structure, whereas symmetric octameric arrangement was observed in *Af*-C3PO structure (Figure 6A and B). Remarkably, although ssRNA (A10) was used for *Ne*-C3PO co-crystallization, the determined crystal structure of *Ne*-C3PO in complex with ssRNA showed that the two ssRNA strands are partially paired and captured next to the interface between the two TRAX–Translin heterodimers (Figure 6B). Comparison of the structures of *Af*-C3PO in complex with dsRNA and *Ne*-C3PO in complex with ssRNA clearly showed that both dsRNA and ssRNA are located at the similar position within the C3PO interior cavity (Figure 6C).

To investigate the structural insights into RNA binding by *Drosophila*-C3PO particle, we made a visualization model of *Drosophila*-C3PO particle in complex with RNA duplex by superimposing the docked octameric *Drosophila*-

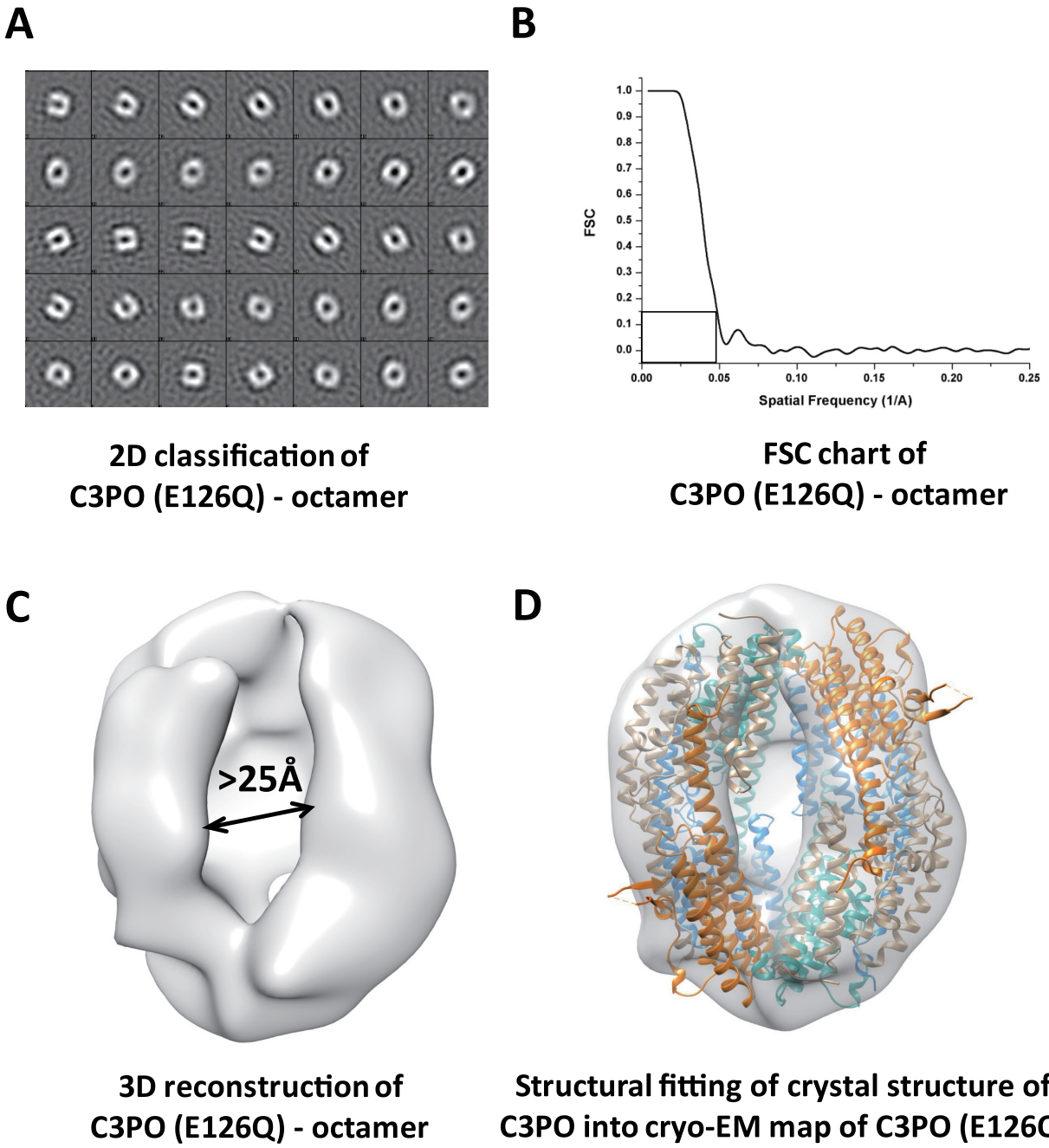

Figure 3. Cryo-electron microscopy and 3D reconstruction of full-length *Drosophila*-C3PO (E126Q) octamer. (**A**) 2D classification of full-length *Drosophila*-C3PO (E126Q) particles derived from EM images collected under 120 kV at 67 000× magnification from Tecnai 12 TEM cryo-electron microscopy. (**B**) The Fourier Shell Correlation curve of resolution between the two independent data sets used for our current reconstruction is shown. The dashed line corresponds to the gold standard criterion for resolution estimate (FSC ∼ 0.143). (**C**) The 3D reconstructed cryo-EM structure of full-length *Drosophila*-C3PO (E126Q) particle with an open side port. (**D**) Structural fitting of full-length crystal structure of C3PO tetramer into the reconstructed ∼19.7 Å C3PO (E126Q) cryo-EM density map. The TRAX subunits are colored in green and orange, respectively, whereas the Translin subunits are colored in blue and yellow respectively. The side port controlling α1 helices from TRAX subunits are colored in red.

C3PO (WT) structure with the structure of *Af*-C3PO in complex with RNA duplex by aligning the characteristic TRAX α1 helices. In our model, a fourteen base-pair RNA duplex is packed along one side of the C3PO inner cavity and the catalytic patches of the head-to-tail packed TRAX–TRAX subunits specifically target opposite strands of the duplex for cleavage (Figure 6D). Moreover, we noticed that although the inner cavity is large enough to encapsulate almost two anti-parallel packed RNA duplexes simultaneously, the negatively charges from the anti-parallel packed RNA duplexes could prevent such close packing (Figure 6E and F). Such observation suggested that *Drosophila*-C3PO particle could only use one of the two TRAX–TRAX centers for RNA substrate binding and cleavage at one time.

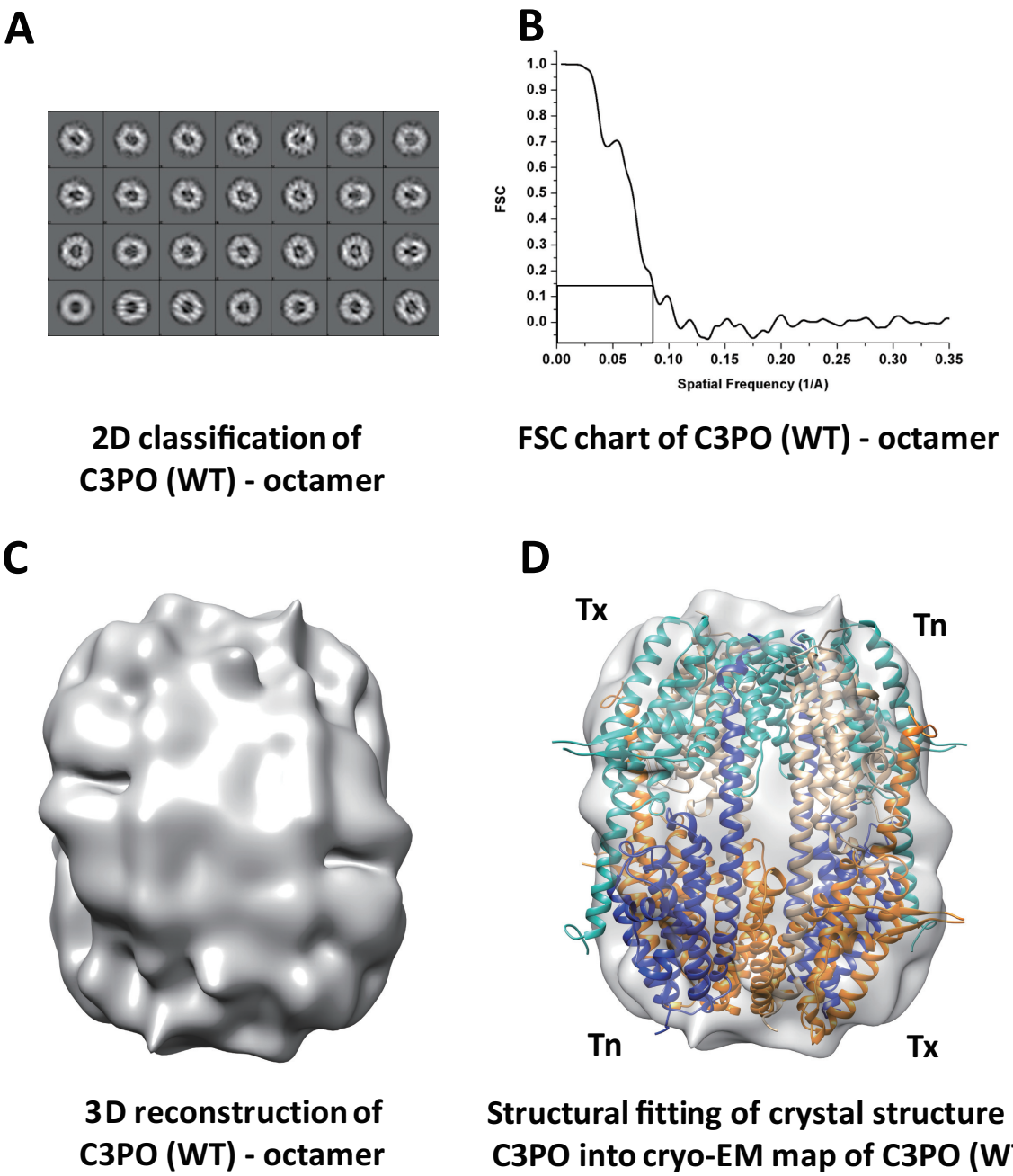

Figure 4. Cryo-electron microscopy and 3D reconstruction of full-length *Drosophila*-C3PO (WT) octamer. (**A**) 2D classification of full-length *Drosophila*-C3PO (WT) particles derived from EM images collected under 120 kV at 67 000× magnification from Tecnai 12 TEM cryo-electron microscopy. (**B**) The Fourier Shell Correlation curve of resolution between the two independent data sets used for our current reconstruction is shown. The dashed line corresponds to the gold standard criterion for resolution estimate (FSC ∼ 0.143). (**C**) The 3D reconstructed cryo-EM structure of full-length *Drosophila*-C3PO (WT) particle. (**D**) Structural docking of full-length crystal structure of C3PO tetramer into the reconstructed ∼12 Å cryo-EM density map of C3PO (WT). The secondary structures of some α-helices are revealed in the map and crystal structures are docked. The TRAX subunits are colored in green and orange, respectively, whereas the Translin subunits are colored in blue and yellow respectively. The side port controlling α1 helices from TRAX subunits are colored in red.

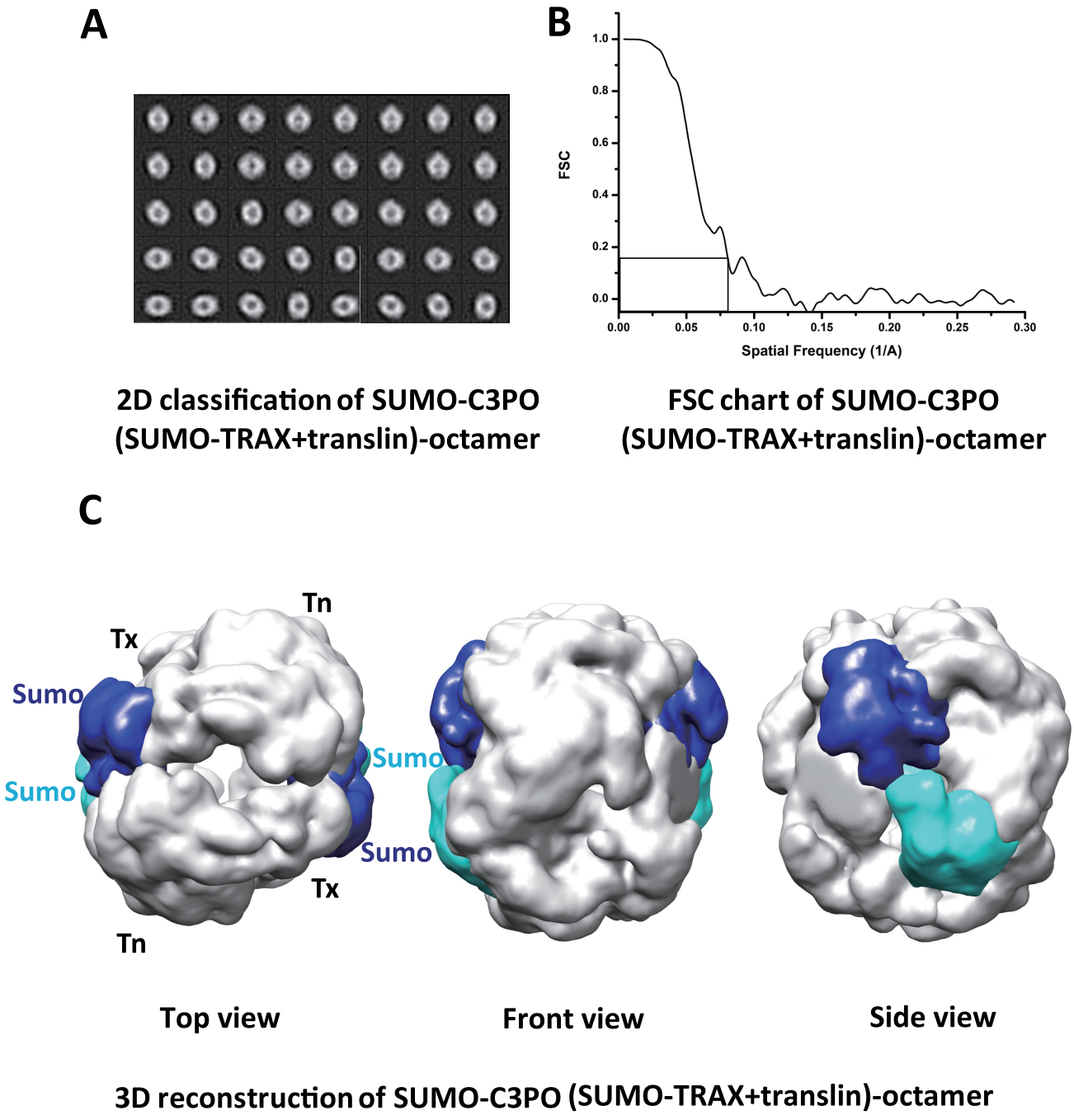

Figure 5. Cryo-electron microscopy and 3D reconstruction of full-length *Drosophila*-SUMO-C3PO (WT) octamer. (**A**) 2D classification of full-length *Drosophila*-SUMO-C3PO (WT) particles derived from EM images collected under 120 kV at 67 000× magnification from Tecnai 12 TEM cryo-electron microscopy. (**B**) The Fourier Shell Correlation curve of resolution between the two independent data sets used for our current reconstruction is shown. The dashed line corresponds to the gold standard criterion for resolution estimate (FSC ∼ 0.143). (**C**) The 3D reconstructed cryo-EM structure of full-length *Drosophila*-SUMO-C3PO (WT) particle in top view, front view and side view, respectively.

Consistently, our *Drosophila*-C3PO (E126Q) particle reveals only one side port under the cryo-EM condition (Figure 3C). We speculate the alternative closing and opening one side port regulated by TRAX–TRAX subunits could be a unique mechanism not only for *Drosophila*-C3PO to take up RNA substrate and release RNA fragment but also for other C3PO octamers. Consistently, cryo-EM structure of human-C3PO also showed only one side port (8).

DISCUSSION

Multimeric assembly of *Drosophila*-C3PO

In literature, different TRAX: Translin ratios were proposed based on the crystal structural analysis, chromatographic analysis, mass spectrometric analysis etc (23). In addition, homo-octamers were reported for human Translin and *Af*-C3PO (24,29). Surprisingly, *in vitro* expressed *Drosophila*-

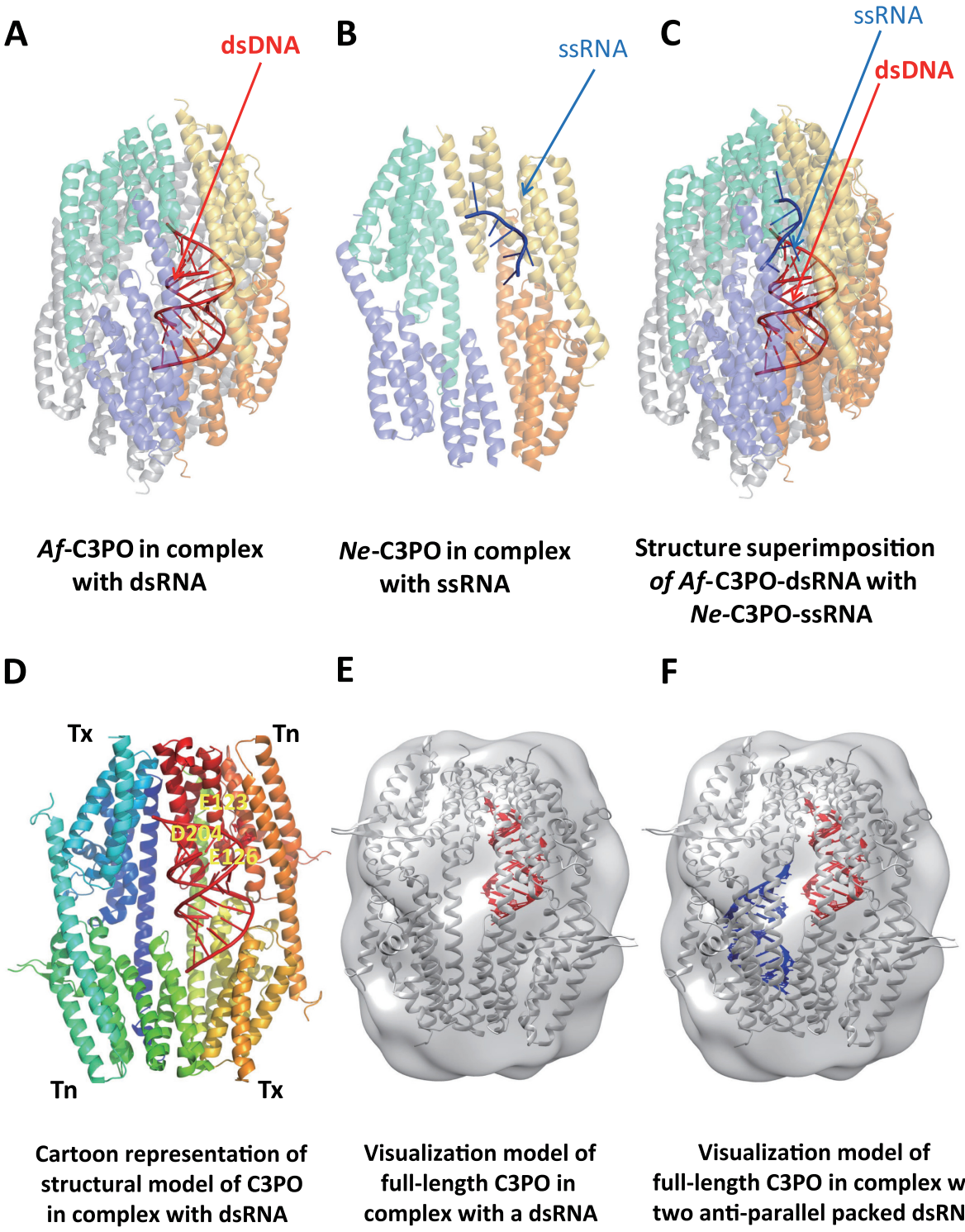

Figure 6. Crystal structures of C3PO in complex with nucleic acids. (**A**) Cartoon representation of crystal structure of *Archaeoglobus fulgidus* C3PO (*Af*-C3PO) in complex with dsRNA. The bound nucleic acids are represented in stick mode and colored in red. (**B**) Cartoon representation of crystal structure of *Nanoarchaeum equitans* C3PO (*Ne*-C3PO) in complex with ssRNA. (**C**) Structural superimposition of *Af*-C3PO in complex with dsRNA and *Ne*-C3PO in complex with ssRNA. *Af*-C3PO in complex with dsRNA colored in light red, whereas *Ne*-C3PO is colored in light blue. The bound nucleic acids are represented in stick mode. (**D**) Cartoon representation of visualization structural model of full-length *Drosophila*-C3PO particle in complex with dsRNA derived from structural superimposition of structures of *Drosophila*-C3PO particle with *Af*-C3PO in complex with dsRNA. The bound dsRNA is represented in stick mode and the catalytic residues are indicated. (**E**) Visualization model of full-length *Drosophila*-C3PO in complex with a single dsRNA. The full-length *Drosophila*-C3PO structure is presented by the Cryo-EM density map and the bound dsRNA is presented in stick mode. (F) Visualization model of full-length *Drosophila*-C3PO in complex with two anti-parallel packed dsRNAs. This model is derived from the structural superimposition of full-length *Drosophila*-C3PO particle structure with *Af*-C3PO in complex with dsRNA at two directions. The *Drosophila*-C3PO particle structure is presented by the Cryo-EM density map and the two bound dsRNA duplexes are presented in stick mode.

C3PO contains two major components comprising 2:4 and 2:2 TRAX–Translin species, and either 3:5 or 2:6 ratio (TRAX–Translin) was proposed for *Drosophila*-C3PO EM structure (21,23). Such data strongly suggested that at least *in vitro* expressed *Drosophila*-C3PO could contain different complexes with varied numbers of TRAX–Translin heterodimers and Translin–Translin homodimers. Notably, more extensive hydrophobic interactions are observed between TRAX–Translin heterodimer than Translin–Translin homodimer. Moreover, the correct folding of TRAX depends on the co-expression of Translin since the expression of TRAX alone yields incorrect folding, suggesting that TRAX–Translin might be expressed as pairs if both TRAX and Translin are available. Therefore, the asymmetric octameric fold, which contains either two TRAX–Translin heteromers, coupled with two Translin–Translin homodimers or three TRAX–Translin heteromers, coupled with one Translin–Translin homodimers, could be unusual and surprising. Hence, we speculated that such unusual asymmetric arrangement could be an artifact derived from the relatively less expressed TRAX by the *in vitro* co-expression system. In our crystal structure, we observed two TRAX–Translin heterodimers, which form a half-barrel-like architecture with two Translin molecules packed side by side, bracketed by the two TRAX molecules at both sides. Consistently, our SDS-PAGE experiments showed that *in vitro* expressed and assembled *Drosophila*-C3PO after size-exclusion purification displays the equal protein expression levels of TRAX and Translin subunits (Supplementary Figure S6A–D). Moreover, our cryo-EM structures of full-length *Drosophila*-C3PO particle at ∼12 Å resolution showed that C3PO is indeed assembled by four copies of TRAX–Translin homodimers, which was supported by the unique long loop region between α4 and α5 structure of TRAX during structural docking (Figure 4D, Supplementary Figure S5). Remarkably, our cryo-EM structure of full-length *Drosophila*-SUMO-C3PO particle determined at ∼12.8 Å resolution showed that C3PO is indeed assembled by four copies of TRAX–Translin heterodimers, which was supported by the visualization of four copies of extra densities corresponding to the N-terminal SUMO tags on TRAX (Figure 5C).

In our cryo-EM structure, *Drosophila*-C3PO particle contains four TRAX–Translin heterodimers, which are further divided into two groups of tetramers comprising two TRAX–Translin heterodimers. Notably, by comparison of cryo-EM structures of *Drosophila*-C3PO at three different conformations (one with side-port trapped at 'closed conformation' and two with side port trapped at 'open conformation'), we noticed that the two adjacent TRAX molecules could be rotated/shifted to open the side port (Figure 7A–C). Such observation suggested the relative independence of the two tetramers. We further speculated that the tetramer comprising two TRAX–Translin heterodimers could be the building unit for C3PO assembly and the two half barrel-shaped tetramers could be assembled through the head-to-tail packing of TRAX subunits probably triggered by RNA substrate binding. The fully assembled C3PO contains a permanent interior cavity for RNA substrate binding and a transiently opening side port serving as a substrate entry and release pathway. Notably, since football-like C3PO and Translin octamer perform multiple functions in addition to promote RISC assembly; the cleavage activity displayed by TRAX could be separated from those performed by Translin. Hence the interior cavity of C3PO could harbors multiple nucleic acids binding sites in addition to RNA duplex binding site, which is supported by crystal structure of *Ne*-C3PO in complex with nucleic acid substrates (21).

'Dynamic Side Port' model for substrate entry and release

Crystal structures of *Af*-C3PO in complex with dsRNA and *Ne*-C3PO in complex with ssRNA demonstrated that the bound RNA substrates are captured in the interior cavity of the closed football-like shape structures (8,21). Hence, the detailed mechanisms of closed football-like C3PO taking up and releasing the RNA substrate could be the key issue to understand C3PO's function in promoting RISC activity. In literature, both 'dissociation and reassembly' and 'conformational switching' models are proposed (21,24). The 'dissociation and reassembly' model was partially supported by the existence of *Drosophila* Translin tetramer (18), whereas the 'conformational switching' model was supported by the structural comparison of *Ne*-C3PO with and without ssRNA binding (21). However, the marginal conformational change, only ∼17 Å gap between the long α1 helix backbone observed from *Ne*-C3PO structure, could be merely crystal packing or structural 'breathing' (Supplementary Figure S3E). Indeed, similar structural 'breathing' was also reported by comparison of human Translin homo-octamer structures trapped at different conformations (8). Nevertheless, the long α1 helix of TRAX or Translin seems quite flexible and structural bending in the middle of the α1 helices are repeatedly observed (8,21–24,29).

Notably, we found that *Drosophila*-C3PO (E126Q) forms a tetramer comprising two symmetric related TRAX–Translin heterodimers in crystal, while forms an octamer harboring a huge side port (∼25 Å × ∼30 Å) under cryo-EM condition (Figure 3C–D). Surprisingly, using the same condition, *Drosophila*-C3PO (WT) particle forms a closed football-like octamer conformation (Figure 4C and D). Hence, the partial disruption of RNA binding by introduction of E126Q mutation at the substrate-binding site could significantly change the structure of assembled C3PO. The structural comparison of cryo-EM structures of *Drosophila*-C3PO (E126Q) and *Drosophila*-C3PO (WT) reveals the significant structural change of *Drosophila*-C3PO, suggesting the side port could be a RNA substrate entry and release pathway. Moreover, given *Drosophila*-C3PO (E126Q) displays compromised RNA binding ability, the 'side port open' conformation of *Drosophila*-C3PO (E126Q) could represent the structure of *Drosophila*-C3PO particle before RNA substrate capturing, whereas the closed football-like conformation of *Drosophila*-C3PO could present the structure of *Drosophila*-C3PO particle after RNA substrate binding.

Notably, the long α1 helices from the adjacent packed TRAX subunits function as a controlling gate to open and close the side port to facilitate taking up RNA substrates and releasing out the digested RNA fragments. Moreover, the size of the side port discovered by our cryo-EM structure of *Drosophila*-C3PO (E126Q) is ∼25 Å × ∼30 Å, which

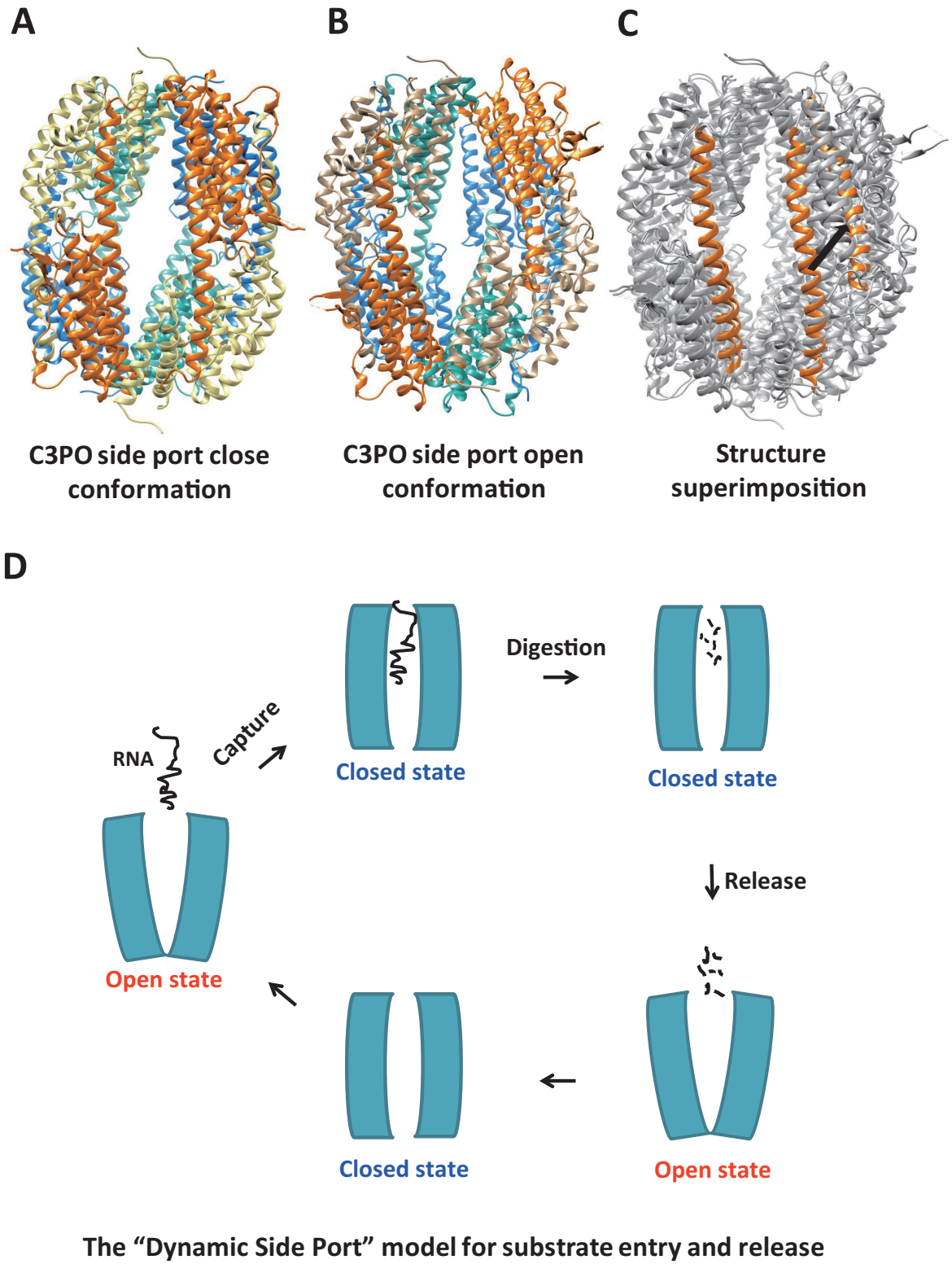

Figure 7. The 'Dynamic Side Port' model for substrate entry digestion and release. (**A**) Structural model of full-length *Droshophila*-C3PO particle at 'side port open' conformation. (**B**) Structural model of full-length *Droshophila*-C3PO particle at 'side port closed' conformation. (**C**) Structural superimposition of full-length *Droshophila*-C3PO particle structures at 'side port open' and 'side port closed' conformations. The structure of full-length *Droshophila*-C3PO particle structure at 'side port open' conformation is colored in grey, whereas the structure of full-length *Droshophila*-C3PO particle structure at 'side port closed' conformation is colored in light blue. The pair of α1 helices regulating the side port opening and closing are colored in orange. (**D**) The proposed 'Dynamic Side Port' model for substrate entry, digestion and release within C3PO chamber. The binding of RNA substrate triggers the conformational rearrangement of C3PO by switching from the 'side port open' conformation to the 'side port closed' conformation. After RNA substrate digestion within the closed C3PO chamber, the side port is open to release the digested nucleic acid fragments.

is wider enough to take up an A-form RNA duplex (∼18 Å in diameter) by multiple directions (Figure 3C). Moreover, we further notice that the size of the side port is quite dynamic by comparison of the cryo-EM structures of *Drosophila* C3PO and *Drosophila* SUMO-C3PO (Figures 4D, 5C and Supplementary Figure S7). Hence, structural comparison of the cryo-EM structures of *Drosophila*-C3PO particles (E126Q versus WT versus SUMO-tagged) trapped at different conformations have provided the direct evidence to explain how C3PO particle recruits/releases nucleic acids into/out the interior of a closed football-like chamber. In addition, structural comparison of crystal structure of *Drosophila*-C3PO (E126Q) and cryo-EM structures of *Drosophila*-C3PO particles (E126Q versus WT versus SUMO-tagged) strongly suggests that oligomeric state of C3PO could be more dynamic in solution than expected, probably due to the weak interactions between TRAX subunits and the possible roles of nucleic acids played in C3PO assembly. Notably, the depletion of nucleic acids binding could favor tetramer formation, while disfavor C3PO assembly into a closed football-like shape. Consistent to this hypothesis, the introduction of a point mutation in human Translin protein lead to tetramer formation with a lower ss-DNA binding affinity (26).

Furthermore, the 2D average cryo-EM images of *Drosophila*-C3PO (E126Q) showed two dominant conformations: one displaying an open conformation with a side port and the other displaying a closed football-like shape (Figure 3A). Remarkably, the percentage of *Drosophila*-C3PO (E126Q) particles containing side port conformation can be significantly increased after the junk nucleic acids are stringently removed during purification (Figure 3A and data not shown). Such observation strongly suggested that nucleic acids binding may stabilize the football-like shape conformation and function as the key component for functional *Drosophila*-C3PO particle assembly. We suggested that without nucleic acids binding, *Drosophila*-C3PO is at a structural 'breathing' mode with side port opening at either side, regulated by a pair of long α-helices from anti-parallel packed TRAX–TRAX dimer. We speculated that the opening of two side ports at the same time could yield the disassembly of *Drosophila*-C3PO into two separated tetramers due to few interactions maintained among *Drosophila*-C3PO subunits, which could be the case as observed by our crystal structure of *Drosophila*-C3PO tetramer. Consistent to this hypothesis, our 2D average images showed majority of *Drosophila*-C3PO (E126Q) particles depletion of nucleic acids binding adopt a side port conformation (Figure 3A). We further suggested that the capture/release of nucleic acids *Drosophila*-C3PO interior chamber could trigger the opening/closing of the dynamic side port by regulating local conformational changes around α1 helices of the packed TRAX–TRAX. (Figure 7D).

Hence, our 'Dynamic Side Port' model could explain RNA substrate capture, digestion and release by assembled *Drosophila*-C3PO octamer. Given the similar structural fold of assembled Translin family proteins, the 'Dynamic Side Port' model may also be applied to explain the molecular mechanism of assembled Translin octamer in nucleic acids binding and releasing.

DATA AVAILABILITY

Atomic coordinates and structure factors for *Drosophila*-C3PO (E126Q) have been deposited with the Protein Data bank under accession number 3AXJ. The cryo-EM structures of *Drosophila*-C3PO (E126Q), *Drosophila*-C3PO (WT) and *Drosophila*-SUMO-C3PO (WT) have been deposited to EMDB with the accession codes EMDB-6723, EMDB-6722 and EMDB-6899, respectively.

SUPPLEMENTARY DATA

Supplementary Data are available at NAR Online.

ACKNOWLEDGEMENTS

We would like to acknowledge the staff at Cryo-Electron Microscopy Facility at CBIS/NUS for technical assistance and the supporting staff at Shanghai Synchrotron Radiation Facility (U17, SSRF) for assistance in data collection. *Author Contributions*: X.M., X.Y. and Y.A.Y. participated in experimental design and data analysis. X.M., X.Y. and Y.A.Y. carried out the experiments. Y.A.Y. and X.M. wrote the manuscript. All authors read and approved the final manuscript.

FUNDING

Academic Research Fund from Singapore Ministry of Education [MOE2013-T2-2-124]; National University of Singapore (Suzhou) Research Institute (to Y.A.Y.). Funding for open access charge: Academic Research Fund from Singapore Ministry of Education [MOE2013-T2-2-124].
Conflict of interest statement. None declared.

REFERENCES

1. Guo,W., Liew,J.Y. and Yuan,Y.A. (2014) Structural insights into the arms race between host and virus along RNA silencing pathways in Arabidopsis thaliana. *Biol. Rev. Camb. Philos. Soc.*, **89**, 337–355.
2. Wang,Y., Sheng,G., Juranek,S., Tuschl,T. and Patel,D.J. (2008) Structure of the guide-strand-containing argonaute silencing complex. *Nature*, **456**, 209–213.
3. Wang,Y., Juranek,S., Li,H., Sheng,G., Wardle,G.S., Tuschl,T. and Patel,D.J. (2009) Nucleation, propagation and cleavage of target RNAs in Ago silencing complexes. *Nature*, **461**, 754–761.
4. Kaya,E. and Doudna,J.A. (2012) Biochemistry. Guided tour to the heart of RISC. *Science*, **336**, 985–986.
5. MacRae,I.J., Ma,E., Zhou,M., Robinson,C.V. and Doudna,J.A. (2008) In vitro reconstitution of the human RISC-loading complex. *Pro. Natl. Acad. Sci. U.S.A.*, **105**, 512–517.
6. Preall,J.B. and Sontheimer,E.J. (2005) RNAi: RISC gets loaded. *Cell*, **123**, 543–545.
7. Drinnenberg,I.A., Weinberg,D.E., Xie,K.T., Mower,J.P., Wolfe,K.H., Fink,G.R. and Bartel,D.P. (2009) RNAi in budding yeast. *Science*, **326**, 544–550.
8. Ye,X., Huang,N., Liu,Y., Paroo,Z., Huerta,C., Li,P., Chen,S., Liu,Q. and Zhang,H. (2011) Structure of C3PO and mechanism of human RISC activation. *Nat. Struct. Mol. Biol.*, **18**, 650–657.
9. Gregory,R.I., Chendrimada,T.P., Cooch,N. and Shiekhattar,R. (2005) Human RISC couples microRNA biogenesis and posttranscriptional gene silencing. *Cell*, **123**, 631–640.
10. Ameres,S.L., Martinez,J. and Schroeder,R. (2007) Molecular basis for target RNA recognition and cleavage by human RISC. *Cell*, **130**, 101–112.
11. Ma,J.B., Yuan,Y.R., Meister,G., Pei,Y., Tuschl,T. and Patel,D.J. (2005) Structural basis for 5′-end-specific recognition of guide RNA by the A. fulgidus Piwi protein. *Nature*, **434**, 666–670.

12. Finkenstadt,P.M., Jeon,M. and Baraban,J.M. (2002) Trax is a component of the Translin-containing RNA binding complex. *J. Neurochem.*, **83**, 202–210.
13. Kim,V.N., Han,J. and Siomi,M.C. (2009) Biogenesis of small RNAs in animals. *Nat. Rev. Mol. Cell Biol.*, **10**, 126–139.
14. Carthew,R.W. and Sontheimer,E.J. (2009) Origins and Mechanisms of miRNAs and siRNAs. *Cell*, **136**, 642–655.
15. Tomari,Y., Matranga,C., Haley,B., Martinez,N. and Zamore,P.D. (2004) A protein sensor for siRNA asymmetry. *Science*, **306**, 1377–1380.
16. Kawamata,T. and Tomari,Y. (2010) Making RISC. *Trends Biochem. Sci.*, **35**, 368–376.
17. Claussen,M., Koch,R., Jin,Z.Y. and Suter,B. (2006) Functional characterization of Drosophila Translin and Trax. *Genetics*, **174**, 1337–1347.
18. Aoki,K., Ishida,R. and Kasai,M. (1997) Isolation and characterization of a cDNA encoding a Translin-like protein, TRAX. *FEBS Lett.*, **401**, 109–112.
19. Aoki,K., Suzuki,K., Sugano,T., Tasaka,T., Nakahara,K., Kuge,O., Omori,A. and Kasai,M. (1995) A novel gene, Translin, encodes a recombination hotspot binding protein associated with chromosomal translocations. *Nat. Genet.*, **10**, 167–174.
20. Gupta,G.D., Kale,A. and Kumar,V. (2012) Molecular evolution of translin superfamily proteins within the genomes of eubacteria, archaea and eukaryotes. *J. Mol. Evol.*, **75**, 155–167.
21. Zhang,J., Liu,H., Yao,Q., Yu,X., Chen,Y., Cui,R., Wu,B., Zheng,L., Zuo,J., Huang,Z. *et al.* (2016) Structural basis for single-stranded RNA recognition and cleavage by C3PO. *Nucleic Acids Res.*, **44**, 9494–9504.
22. Li,L., Gu,W., Liang,C., Liu,Q., Mello,C.C. and Liu,Y. (2012) The translin-TRAX complex (C3PO) is a ribonuclease in tRNA processing. *Nat. Struct. Mol. Biol.*, **19**, 824–830.
23. Tian,Y., Simanshu,D.K., Ascano,M., Diaz-Avalos,R., Park,A.Y., Juranek,S.A., Rice,W.J., Yin,Q., Robinson,C.V., Tuschl,T. *et al.* (2011) Multimeric assembly and biochemical characterization of the Trax-translin endonuclease complex. *Nat. Struct. Mol. Biol.*, **18**, 658–664.
24. Parizotto,E.A., Lowe,E.D. and Parker,J.S. (2013) Structural basis for duplex RNA recognition and cleavage by Archaeoglobus fulgidus C3PO. *Nat. Struct. Mol. Biol.*, **20**, 380–386.
25. Eliahoo,E., Marx,A., Manor,H. and Alian,A. (2015) A novel open-barrel structure of octameric translin reveals a potential RNA entryway. *J. Mol. Biol.*, **427**, 756–762.
26. Liu,Y., Ye,X., Jiang,F., Liang,C., Chen,D., Peng,J., Kinch,L.N., Grishin,N.V. and Liu,Q. (2009) C3PO, an endoribonuclease that promotes RNAi by facilitating RISC activation. *Science*, **325**, 750–753.
27. Terwilliger,T.C. and Berendzen,J. (1999) Automated MAD and MIR structure solution. *Acta Crystallogr. D, Biol. Crystallogr.*, **55**, 849–861.
28. Gomez-Escobar,N., Almobadel,N., Alzahrani,O., Feichtinger,J., Planells-Palop,V., Alshehri,Z., Thallinger,G.G., Wakeman,J.A. and McFarlane,R.J. (2016) Translin and Trax differentially regulate telomere-associated transcript homeostasis. *Oncotarget*, **7**, 33809–33820.
29. Sugiura,I., Sasaki,C., Hasegawa,T., Kohno,T., Sugio,S., Moriyama,H., Kasai,M. and Matsuzaki,T. (2004) Structure of human translin at 2.2 A resolution. *Acta Crystallogr. D, Biol. Crystallogr.*, **60**, 674–679.